Proceedings of 3rd International Civil Engineering and Architecture Congress (ICEARC'23)
DOI 10.31462/icearc.2023.sme213

Modeling of plane elasto-plastic reinforced concrete frame system with developed finite element algorithm

Semiha Hayrioğlu[1*], Serkan Bekiroğlu[1]

[1] Yıldız Technical University, Department of Civil Engineering, İstanbul, Türkiye

Abstract

Purpose: A nonlinear material model for concrete and reinforcement was created in order to establish numerical models of two-dimensional reinforced concrete membrane problems.
Study design/methodology/approach: Based on the Druker-Prager model for the concrete material, the hardening zone is defined as a multi-part linear curve. The open region of the conical yield surface is covered with a circular cap in the p-q plane. The Mander concrete model curve, which was expressed in TBEC-2018, was chosen as the concrete stress-strain curve. When the plastic strain begins to occur, Poisson's ratio, dilation rate, cohesion, shear modulus, tangent modulus, elasticity modulus and secant elasticity modulus are updated to follow the Mander curve. The reinforcement is considered as a linear elastic, perfect plastic material model according to the von-Mises criterion. A finite element modeling program was developed using the MATLAB programming language in order to define the materials and provide the solution of the system.
Findings: Finite element modeling program developed in line with the obtained data; until the end of hardening, it provides reasonably consistent results, not only at the force-displacement level, but also at the stress-strain, neutral axis depth and damage level levels, without the need for any further analysis and research on the value of the parameters for validation used in the definition of the concrete material.
Originality/value: The values updated to follow the Mander concrete model curve were quite effective in the consistency of results.

Keywords: A Capped Drucker-Prager Model; Hardening In Concrete; Mander Concrete Model; Dilation Rate; Damage Parameter

1. Introduction

In this study, it is aimed to develop a program that will enable the creation of nonlinear material models in reinforced concrete elements by using the finite element method and the elasto-plastic analysis of the system using appropriate yield criteria with a definition in which material parameters consistent with material curves are obtained following the entire material curve.

Von Mises model for reinforcement material and Drucker Prager model for concrete material was chosen to be used to model reinforced concrete elements.

Mander et al. (1988) developed a unified stress-strain model for confined concrete for members with either circular or rectangular sections, under static or dynamic loading, either monotonically or cyclically applied. The Mander concrete model curve, which was expressed in TBEC-2018, was chosen as the concrete stress-strain curve.

* Corresponding author (semihahayrioglu@gmail.com)
© 2023 Authors. Publishing services by golden light publishing®.
This is an open-access article under the CC BY-NC-ND license (http://creativecommons.org/licenses/by-nc-nd/4.0/).

When the studies conducted on the basis of the main headings mentioned above are examined, in general numerical models; for concrete material, it is understood that the Drucker-Prager model is used with different concrete curvatures, the hardening situation is taken into account, the concrete curves are mostly defined as two-line and the reinforcement is generally defined without hardening. It is understood from the literature research that the results for some material parameters in the models related to the concrete used are very sensitive from a mathematical point of view, therefore, those parameters must be studied numerically in order to capture the results obtained from the experimental study. In the studies carried out, comparisons are usually made with experimental results on load-displacement, and comparisons made on stress-strain remain in the minority. For this purpose, cantilever beam and a portal frame problems are solved in the plane, in order to exemplify that it can be used in the performance evaluation of an element over the case that it contains the reinforced concrete section properties described in TBEC-2018. The stress and strain results obtained from the solution are compared with the defined material curves.

2. Methodology

Nonlinear concrete and reinforcement material models were created to define the reinforced concrete section. The concrete model is based on the Drucker-Prager model and the conical yield surface is covered by a circular cap in the p-q plane. The development of the capped yield surface is proportional to the development of the material stress and strain level. This improvement is achieved by obtaining the values of nonlinear material variables (plastic strain factors) from equations that are solved using the Newton Raphson method during the iteration process. At the same time, the hardening region is defined as a multi-part linear curve. Thus, the confinement effect, which has the greatest influence on the non-linear strength of the concrete material, can be taken into account. In addition, for each concrete stress level, the dilation of concrete is allowed to change and the Poisson ratio to change accordingly. Here, the concrete stress-strain curve is considered as the Mander concrete model curve, which is also referred to in TBEC-2018. The reinforcement model was defined using the von Mises criterion. Hardening is not defined in the nonlinear behavior of the reinforcement material.

In the prepared program, MATLAB programming language was used and modeled using the finite element method. The program works by tracing the uniaxial compressive stress-strain curve, which is used as input information of the point stress-strain value pair obtained by transforming the stress-strain tensors obtained for each point in the solved problem domain to effective values. In addition, for each strain point value needed in the program, the tangent modulus, Poisson's ratio, secant elasticity modulus, elasticity modulus, dilation ratio and angle, shear modulus, internal friction angle, cohesion and amount of plastic strain are derived.

In order to control the development of the cap surface in the Drucker Prager model, the initial stress value is calculated based on the amount of strain in the relevant iteration, and the actual stress value in the relevant step is tried to be found. This process is carried out by return mapping algorithms. It is understood that the material maintains its elastic properties when the stress level in the material does not reach the capped yield surface.

2.1.1. The von Mises model

According to the von Mises criterion; for a unit volume, the material begins to flow when the multiaxial strain energy reaches the experimentally obtained uniaxial strain energy. The von Mises criterion is pressure-insensitive, meaning that the hydrostatic pressure component of the stress tensor does not affect the yielding. The yield function and yield surface of the model are given in Eq. 1 and in Fig. 1, respectively.

$$\Phi = \sqrt{3J_2(s)} - \sigma_y(\overline{\varepsilon}_p) \tag{1}$$

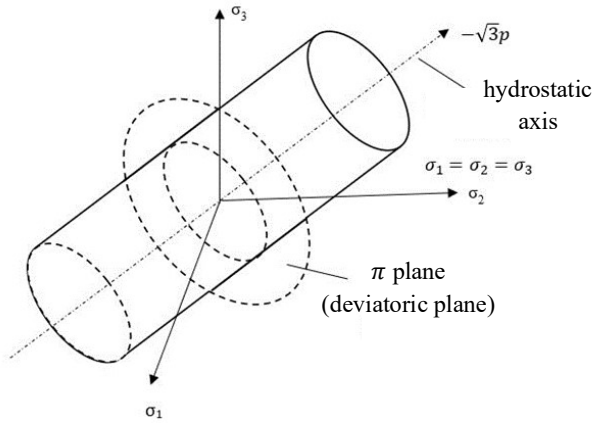


Fig. 1. von Mises yield surfaces in principal stress space

In the Von Mises model, the equivalent plastic strain calculation and effective stress calculation are shown in Eqs. 2-3, respectively.

$$d\varepsilon^p = \sqrt{\frac{2}{3}}\sqrt{d\varepsilon_{ij}^p d\varepsilon_{ij}^p} \tag{2}$$

$$\sigma_{eff} = \sqrt{\sigma_{11}^2 + \sigma_{22}^2 - \sigma_{11}\sigma_{22} + 3\sigma_{12}^2} = \sqrt{\frac{3}{2}s_{ij}s_{ij}} \tag{3}$$

The problems in the study are solved as plane strain problems. In the case of plane strain, the size of the structure in one direction (for example, z) is very large compared to the dimensions in the other two directions. Therefore the deformations in this direction are assumed to be zero.

2.1.2. The capped Drucker-Prager model

The Drucker–Prager yield criterion is a simple modification of the von Mises criterion, in which the hydrostatic stress component is included to ensure pressure sensitivity. The yield function of the Drucker-Prager model is given in Eq. 4.

$$\Phi^a = \sqrt{J_2} + \eta p - \xi c = 0 \tag{4}$$

Here ξ and η are the material parameters. For the plane strain state, the values in the non-associative and associative states are given in the Eqs. 5-7.

$$\xi = \frac{3}{\sqrt{9 + 12\,tan^2\,\phi}} \tag{5}$$

$$\eta = \frac{3\,tan\,\phi}{\sqrt{9 + 12\,tan^2\,\phi}} \tag{6}$$

$$\bar{\eta} = \frac{3\,tan\,\psi}{\sqrt{9 + 12\,tan^2\,\psi}} \tag{7}$$

The addition of a capped yield surface to the Drucker-Prager model serves two main purposes: in hydrostatic compression it limits the yield surface, thus providing an inelastic hardening mechanism to represent plastic compression and it helps to control the volume expansion as the material flows in shear, by

providing softening as a function of the inelastic volume increase that occurs at the Drucker-Prager shear fracture surface as the material flows. The yield surface of the capped Drucker-Prager model is shown in Fig. 2. The tangent of the cap curve coincides with the slope of the conical surface of the Drucker-Prager model.

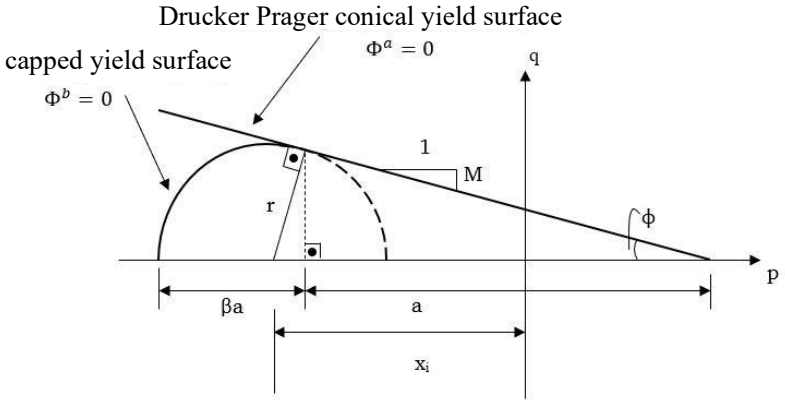


Fig. 2. Capped Drucker-Prager yield surfaces in the p-q plane

The yield function of the capped Drucker-Prager model calculated using the values shown in Fig. 2 is given in Eq. 8.

$$\Phi^b = \frac{1}{\beta^2}(p(\sigma) - x_i)^2 + \left(\frac{q(\sigma)}{\beta}\right)^2 - a^2 \tag{8}$$

The calculation of the β parameter here is as shown in Eq. 9.

$$\beta = M\sqrt{M^2 + 1} \tag{9}$$

Considering that the equivalent plastic strain is a positive quantity and possesses the dimension of strain, the equivalent plastic strain can be defined as in Eq. 10. In the plastic stage, the angle of internal friction ϕ and the cohesion c are no longer constants but do vary with the plastic internal variable (κ). (Ding and Zhang, 2017). The value of the coefficient C is given in the Eq. 11.

$$d\varepsilon^p = C\sqrt{d\varepsilon_{ij}^p d\varepsilon_{ij}^p} \tag{10}$$

$$C(\kappa) = \frac{\sqrt{1/3} + \alpha(\kappa)}{\sqrt{3\left(\alpha(\kappa)\right)^2 + 1/2}} \tag{11}$$

Here, $\alpha(\kappa)$ value is calculated as given in Eq. 12, where α is the pressure sensitivity coefficient and κ is the plastic variable.

$$\alpha(\kappa) = \frac{\eta}{3} \tag{12}$$

The effective stress value developed using the effective stress relations given in Chen W. F. (1982) is calculated as shown in the Eq. 13.

$$\sigma_{eff} = \frac{3\alpha(\kappa)p_{n+1} + \sqrt{J_2(s_{n+1})}}{\alpha(\kappa) + \sqrt{1/3}} \tag{13}$$

2.1.3. Stress-strain relationship of concrete

The stress-strain approach proposed for concrete by Mander et al. (1984) is shown in Fig. 3. Correlations for the Mander model are taken from the Turkish Building Earthquake Code (TBEC, 2018).

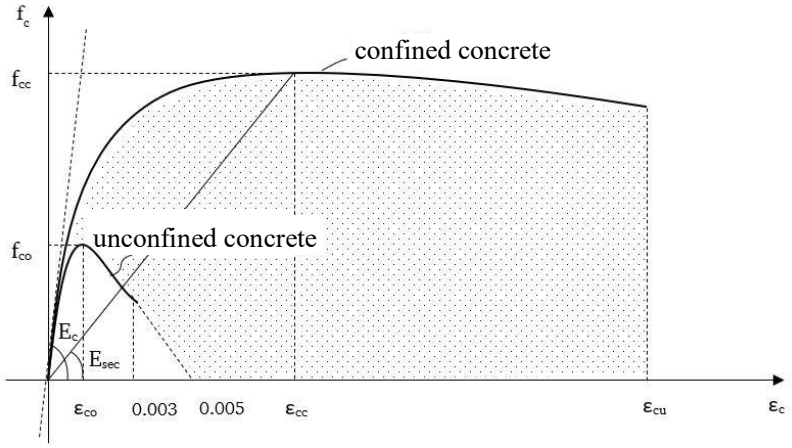


Fig. 3. Recommended stress-strain model for monotonic loading of confined and unconfined concrete

The effective confining pressure f_e is calculated for two perpendicular directions in rectangular sections. In this study, since the rectangular section of the beam is considered and the beams are subjected to bending around a single line, only one direction is taken into account in the calculation of ρ, since the stirrups in the short direction of the beam section will create a containment effect. The calculation of f_e is given in Eq. 14.

$$f_e = k_e \rho f_{yw} \tag{14}$$

Here f_{yw} is the yield strength of the transverse reinforcement, ρ given in Eq. 15 is the volumetric ratio of the total transverse reinforcement and k_e in Eq. 16 is the confinement efficiency coefficient ratio. Dimensions in the reinforced concrete section are shown in Fig. 4.

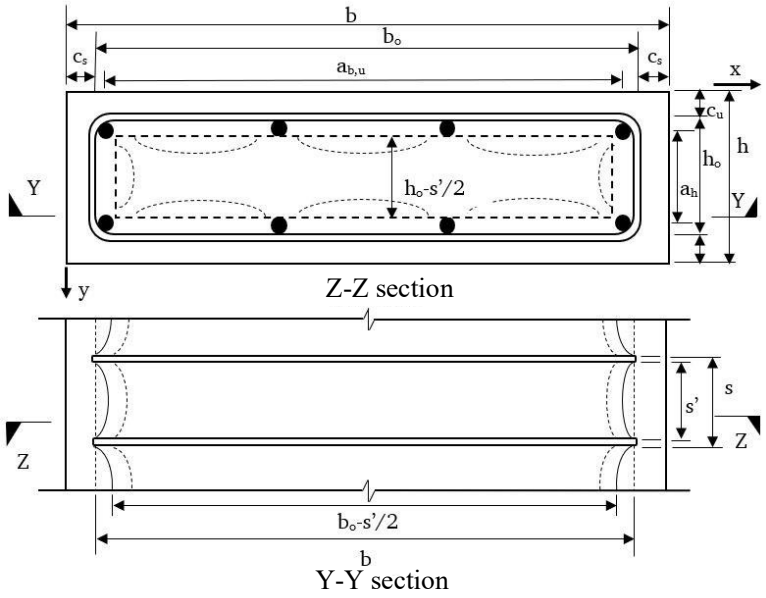


Fig. 4. Dimensions of confined concrete

$$\rho = \frac{2(h_o + b_o){d_t}^2 \frac{\pi}{4}}{h_o b_o s} = \frac{(h_o + b_o)d_t^2 \pi}{2h_o b_o s} \tag{15}$$

$$k_e = \left(1 - \frac{\sum a_i^2}{6b_o h_o}\right)\left(1 - \frac{s}{2b_o}\right)\left(1 - \frac{s}{2h_o}\right)\left(1 - \frac{A_s}{b_o h_o}\right)^{-1} \tag{16}$$

Where a_i is the distance between adjacent longitudinal reinforcements given in Eq. 18. b_o and c_o are the core dimensions relative to the center lines of the perimeter stirrup in the x and y directions. s is the distance between the centers of the stirrups. A_s in Eq. 17 is the area of the longitudinal reinforcement.

$$A_s = \frac{b_u^2 \pi}{4} b_{u,n} + \frac{b_d^2 \pi}{4} b_{d,n} \tag{17}$$

Where b_u is the diameter of longitudinal reinforcement at the top of a rectangular beam, b_d is the diameter of longitudinal reinforcement at the bottom of a rectangular beam and $b_{u,n}$ and $b_{d,n}$ are the number of these reinforcements.

$$\sum a_i^2 = 2\left[\left(\frac{a_{b,u}}{b_{u,n} - 1}\right)^2 + \left(\frac{a_{b,d}}{b_{d,n} - 1}\right)^2 + {a_h}^2\right] \tag{18}$$

Here, $a_{b,u}$ is the center-to-center distance of the upper longitudinal reinforcement. $a_{b,d}$ is the center-to-center distance of the lower longitudinal reinforcements and a_h is the center-to-center distance of the bottom and top reinforcements along the depth.

2.2. Derivation of values following the stress-strain curve

The uniaxial compressive stress-strain curve, which is the input information, was taken into account as the Mander concrete material curve used in TBEC-2018. In the curve created according to the Mander model, the entire region is divided into sub-regions until the maximum pressure in the confined concrete reaches the strain value when the stress is zero, beyond the unit strain value. The values calculated at each strain point along the curve (including the softening region) are collected in a matrix.

2.2.1. Derivation of the tangent modulus

It is calculated by using the difference between the stress and strain values of the point corresponding to each strain moment and the stress and strain values of the point corresponding to the previous strain moment. This calculation is shown in Eq. 19.

$$E_{t_i} = \frac{f_{c_i} - f_{c_{i-1}}}{\varepsilon_{c_i} - \varepsilon_{c_{i-1}}} \tag{19}$$

2.2.2. Derivation of the Poisson's ratio

In the study, it was assumed that the volumetric strain rate was constant. In this case, since the bulk modulus (K) value is constant, the Poisson's ratio must also change with the changing elasticity modulus value. Considering that the bulk modulus is constant, the equality stated in Eq. 20 is obtained.

$$K = \frac{\sigma_1}{3\varepsilon_1(1 - 2\nu_1)} = \frac{\sigma_i}{3\varepsilon_i(1 - 2\nu_i)} \tag{20}$$

When the Poisson's ratio is taken from here, the formulation given in Eq. 21 is obtained.

$$\nu_i = \frac{1}{2}\left[1 - \frac{\sigma_i \varepsilon_1}{\sigma_1 \varepsilon_i}(1 - 2\nu_1)\right] \tag{21}$$

2.2.3. Derivation of the secant elasticity modulus

The slope of the line drawn from the zero point to the point corresponding to each strain moment in the steps following the Mander curve gives the secant elasticity modulus. The secant elasticity modulus was used to calculate the shear modulus, assuming that all of the damage was plastic. The amount of plastic strain in the calculations is obtained by using the secant elasticity module. The secant elasticity modulus is obtained from the bulk modulus formula given in Eq. 22. It is calculated as shown in Eq. 23.

$$K = \frac{E_s}{3(1 - 2\nu)} \tag{22}$$

$$E_{s_i} = 3K(1 - 2\nu_i) \tag{23}$$

2.2.4. Derivation of the elasticity modulus

Elasticity modulus calculated as shown in Eq. 24. Here, ε_{cu} used in Eq. 26 is the ultimate compressive strain value, ε_{cudr} is the collapse strain value and d calculated in Eq. 25 is the damage parameter.

$$E_e = E_c(1 - d_i) \tag{24}$$

$$d_i = \frac{\varepsilon_{c_i} E_c - f_{c_i}}{\varepsilon_{cud} E_c} \tag{25}$$

$$\varepsilon_{cud} = \varepsilon_{cu} + \varepsilon_{cudr} \tag{26}$$

Due to the nature of the concrete material, the fact that the stress of the concrete is constantly less than the stress caused by the initial elastic modulus and strain actually means that the concrete material develops continuous damage due to strain. In addition, from the relationship between Poisson's ratio and dilation, it is understood from the experimental studies in the literature that the Poisson ratio changes with strain. Therefore, the definition of the stress-strain relationship of the concrete material is based on damage.

The elasticity module defined here is used in calculating the plastic strain value from the total strain value for the stress strain graph obtained by uniaxial testing. Therefore, the definition of elasticity modulus here is defined only for the stress-plastic strain relationship of the material.

2.2.5. Derivation of the damage parameter

When looking at the stress-strain graph of concrete under uniaxial compressive loading (Fig. 5), the plastic strain component of the strain amount corresponding to a point on the graph is calculated depending on the damage parameter. In this regard, the calculated plastic strain amount is compared with the amount of plastic strain obtained as a result of the analysis made with the capped Drucker-Prager model, and it is decided which material parameters derived at the current stage will be used.

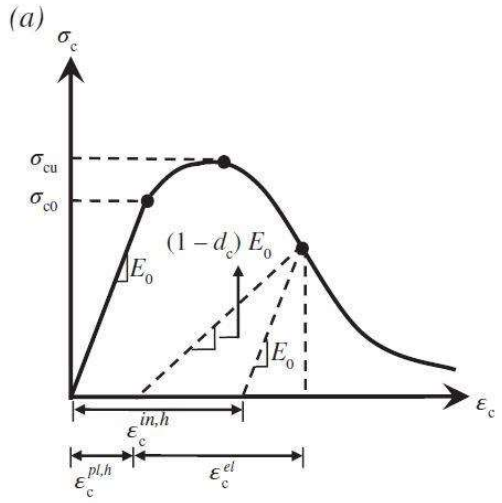


Fig. 5. Response of concrete to a uniaxial loading condition: Compression

2.2.6. Derivation of the dilation rate

Poisson's ratio or the rate of change of radial (lateral) strains with respect to axial strains is called the dilation rate (Mirmiran and Shahawy, 1997). The calculation of the dilation rate is shown in Eq. 27.

$$\mu = \frac{\mu_0 + ax + b^2}{1 + cx + dx^2} \tag{27}$$

Here μ_0=initial dilation rate, x=$\varepsilon_c/\varepsilon_{co}$, ε_{co}= peak strain of unconfined concrete and a, b, c and d are the coefficients given in Eq. 28. First, the initial dilation rate (μ_0) is the same as the Poisson's ratio (ν_0) of unconfined concrete. As microcracks develop, the dilation rate tends to increase.

$$a = \mu_0 c \quad ; \quad b = \mu_u d \quad ; \quad c = -2 \quad ; \quad d = \frac{\mu_{0_{max}}}{\mu_{u_{max}}} \tag{28}$$

Approaching the ultimate strain of unconfined concrete, where concrete has lain itself entirely onto the jacket, the dilation rate reaches a peak value of μ_{max} given in Eq. 29. Once the jacket assumes full control of lateral expansion, dilation rate stabilizes and decreases to an asymptotic value of μ_u (Mirmiran and Shahawy, 1997). The formulation of μ_u is given in Eq. 30.

$$\mu_{max} = -0.7611 Ln\left(\frac{2E_j t_j}{f_c' D}\right) + 4.0167 \tag{29}$$

$$\mu_u = -0.1375 Ln\left(\frac{2E_j t_j}{f_c' D}\right) + 0.8646 \tag{30}$$

($2E_jt_j/f'_{co}D$) is the stiffness of the jacket to that of the concrete core where f'_{co} strength of unconfined concrete. ε_v is volumetric strain or dilation, ε_c is axial strain and ε_r is lateral strain values given in Eqs. 31-33.

$$\varepsilon_v = \varepsilon_c + 2\varepsilon_r \tag{31}$$

$$\varepsilon_c = \varepsilon \tag{32}$$

$$\varepsilon_r = -\nu\varepsilon \tag{33}$$

When the experimental dilation rate is calculated between successive steps, the dilation rate is calculated as shown in Eqs. 34-35.

$$\mu_i = \frac{\Delta\varepsilon_r}{\Delta\varepsilon_c} = \frac{\varepsilon_{r_i} - \varepsilon_{r_{i-1}}}{\varepsilon_{c_i} - \varepsilon_{c_{i-1}}} \tag{34}$$

$$\mu_i = \frac{(-\nu_i\varepsilon_i) - (-\nu_{i-1}\varepsilon_{i-1})}{\varepsilon_i - \varepsilon_{i-1}} = -(i-1)\nu_{i-1} - i\nu_i \tag{35}$$

2.2.7. Derivation of the dilation angle

Dilation angle was used in the calculation of $\bar{\eta}$ and $\bar{\xi}$ parameters used in the nonassociative Drucker Prager material model for plane stress and plane strain conditions. The dilation angle calculation is given in Eq. 36.

$$\tan^{-1}(\mu_i) = \tan^{-1}[-(i-1)\nu_{i-1} - i\nu_i] \tag{36}$$

2.2.8. Derivation of the shear modulus

Shear modulus refers to the material's resistance to shear stress. It is calculated using the secant elasticity module in the prepared program. Its calculation is given in Eq. 37.

$$G_i = \frac{E_{s_i}}{2(1+\nu_i)} \tag{37}$$

2.2.9. Derivation of the internal friction angle

The internal friction angle given in Eq. 38 was used to calculate the η and ξ parameters and cohesion value used in the associative Drucker Prager material model for plane stress and plane strain conditions.

$$\phi_i = \sin^{-1}\frac{f_{c_i} - f_t}{f_{c_i} + f_t} \tag{38}$$

2.2.10. Derivation of the cohesion

The point where the tangent line drawn to the Mohr circles in the Fig. 6, drawn on the principal plane, intersects the y-axis, gives the cohesion value. The calculation of the cohesion value is as given in Eq. 39.

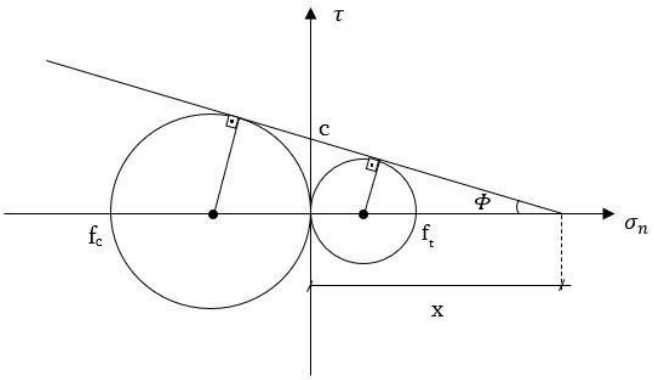


Fig. 6. Mohr circle and failure envelope

$$c_i = \frac{f_{c_i} f_t}{f_{c_i} - f_t} \tan\Phi_i \tag{39}$$

2.2.11. Derivation of the amount of plastic strain

The amount of plastic strain is calculated using the elasticity modulus as in Eq. 40.

$$\varepsilon_i^p = \varepsilon_{c_i} - \frac{f_c}{E_{e_i}} \tag{40}$$

A matrix was created that contains the material parameters mentioned and values of other parameters depending on these parameters in its columns and contains every defined point in its rows.

2.3. Return algorithms in the developed program

In case of plasticization, it is not possible to reach the real yield stress value in a single step. To achieve this, elastic prediction and plastic correction steps are applied. First, the strains at t_n and t_{n+1} steps are assumed to be perfectly elastic. If $\Phi_{trial} \leq 0$ calculated with trial values, that is, if it is in the yield surface or in the elastic region, the assumption made is correct. It is understood that the trial values are real values and the algorithm is terminated. If $\Phi_{trial} > 0$, the elastic prediction loses its validity and a solution is produced with the help of the return mapping algorithm. In the von Mises model, the return is only to the cylindrical yield surface. In the Drucker Prager model, five return algorithms are required to control the development of the defined capped yield surface. These are, in order:

a. return to the smooth portion of the Drucker–Prager cone (First return algorithm)
b. return to the cone apex (Second return algorithm)
c. return to the cap (Third return algorithm)
d. return to the cone/cap intersection (Fourth return algorithm)
e. return to the endpoint of cap (Fifth return algorithm)

Fig. 7 shows the flow diagram of the return mapping process.

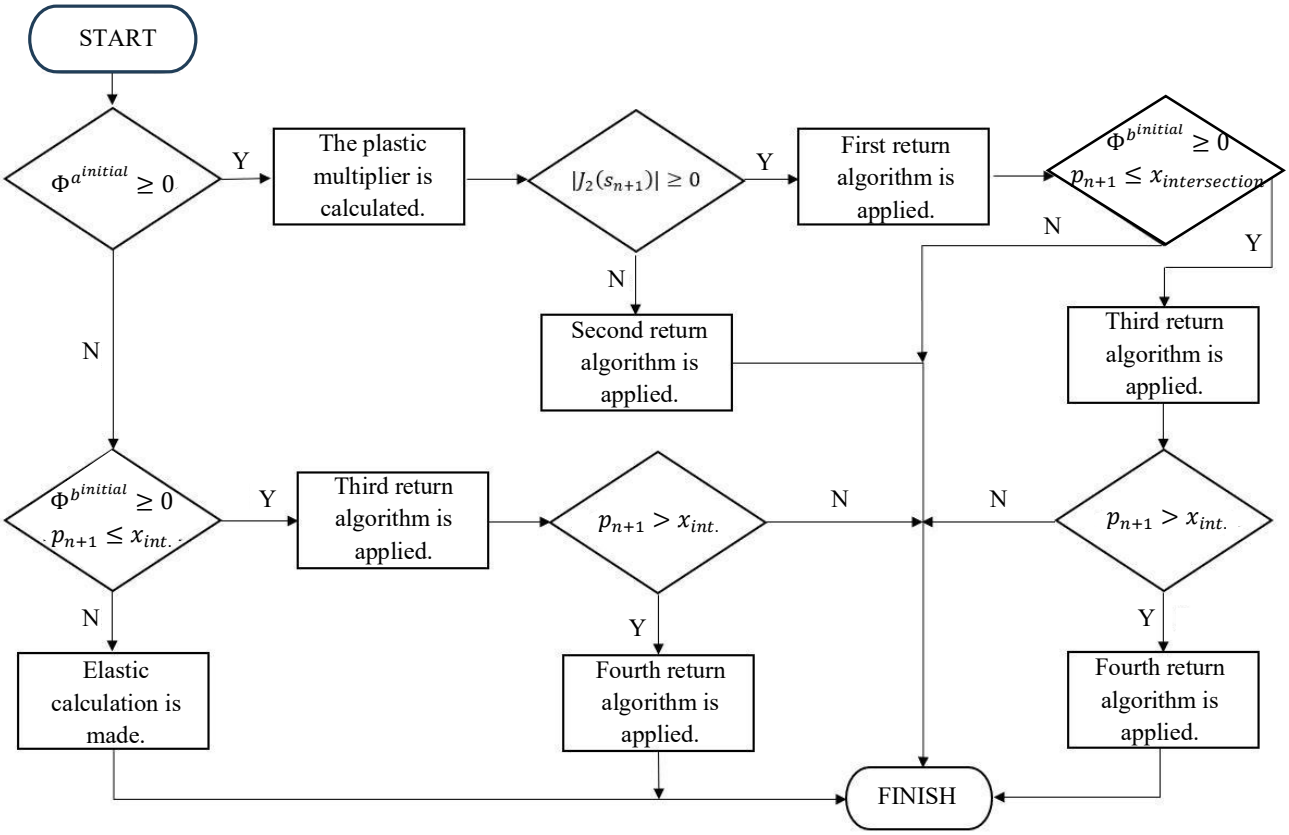


Fig. 7. Flow diagram of return mapping algorithms of the capped Drucker-Prager model

2.4. Sample problems

2.4.1. Reinforced concrete cantilever beam

As an example, a rectangular reinforced concrete cantilever beam with a length of 6000 mm, a height of 500 mm and a width of 250 mm was chosen to be analyzed. Reinforcement and concrete material properties are shown in Table 1.

Table 1. An example representation from the concrete material model in the solved examples

Parameter	Reinforcement steel (von Mises model)	Concrete (Drucker-Prager model)
Elasticity modulus (E) (N/mm^2)	200000	25000
Poisson's ratio (ν)	0,3	0,2
Tangent elasticity modulus (ET) (N/mm^2)	0,0	25000
Yield strength (σ_y) (N/mm^2)	220	f_{cc}
Tensile yield strength (f_t) (N/mm^2)	0,0	f_{tt}

4 pieces of reinforcement with a diameter of 20 mm were used and this beam, shown in Fig. 8, was modeled with rectangular finite elements consisting of 840 elements and 912 node points, using the finite element method. The beam was loaded with a single load of 35000N from its free end (node number 912).

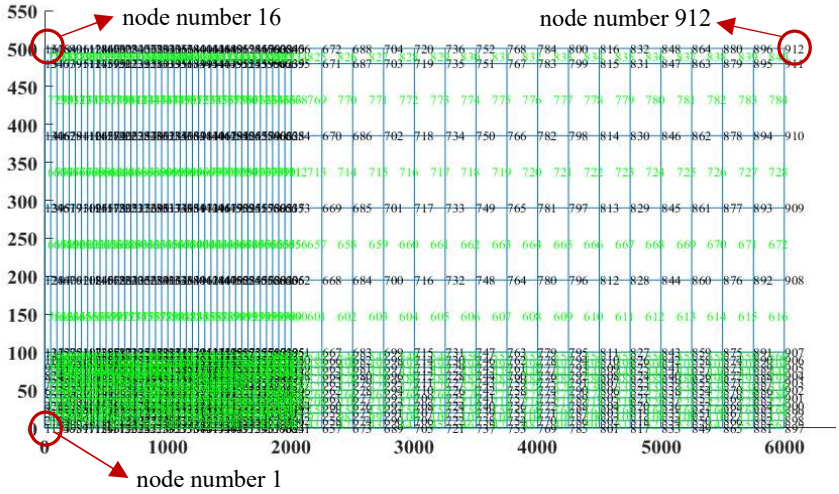


Fig. 8. Finite element modeling of cantilever beam

In the prepared program, the capped Drucker Prager yield surface for the cantilever beam example is created as shown in Fig. 9. As can be seen from the figure, it is seen that the flow surface expands as moving along the material line. At the same time, during the plastic correction steps, the returns to the yield surface of the cap region are observed.

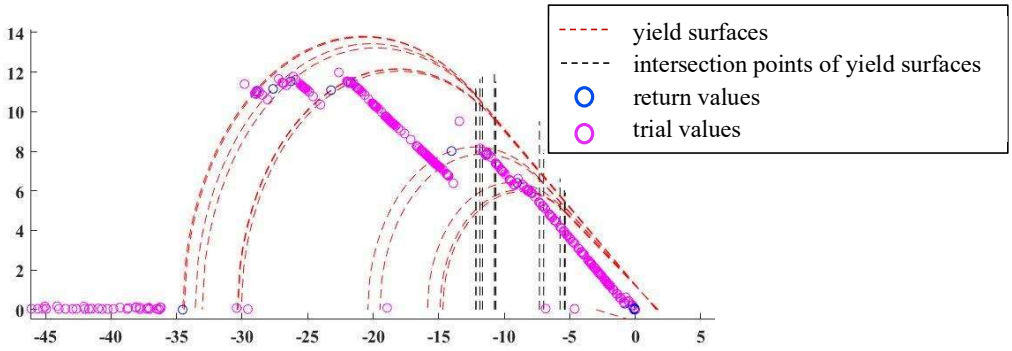


Fig. 9. Capped Drucker-Prager yield surface for cantilever beam

The stress distributions of the cantilever beam analyzed with the specified loading are shown in Fig. 10. In order to easily observe the amount of displacement in deformed shapes, ten times the size was used when plotting the vertical deformations.

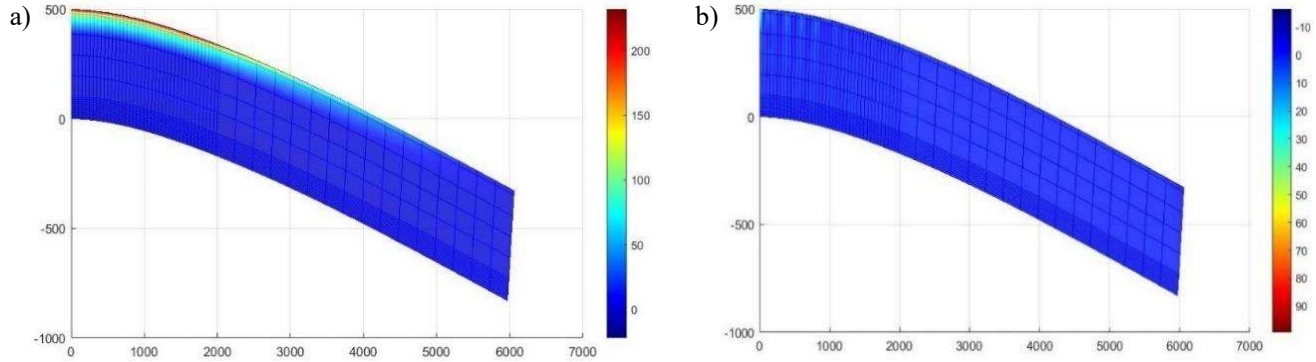


Fig. 10. a) Stress distribution in the x-axis direction of the cantilever beam, b) stress distribution in the y-axis direction of the cantilever beam

As a result, the variation of the stress (Fig. 11), plastic strain (Fig. 12a), total strain (Fig. 12b) and von Mises stress (Fig. 12c) at the node points 1 and 16 of the system at the fixed end (Fig. 8) depending on the iterations is shown in the graphs below. Red color represents the concrete element (node number 1) and blue color represents the reinforcement element (node number 16).

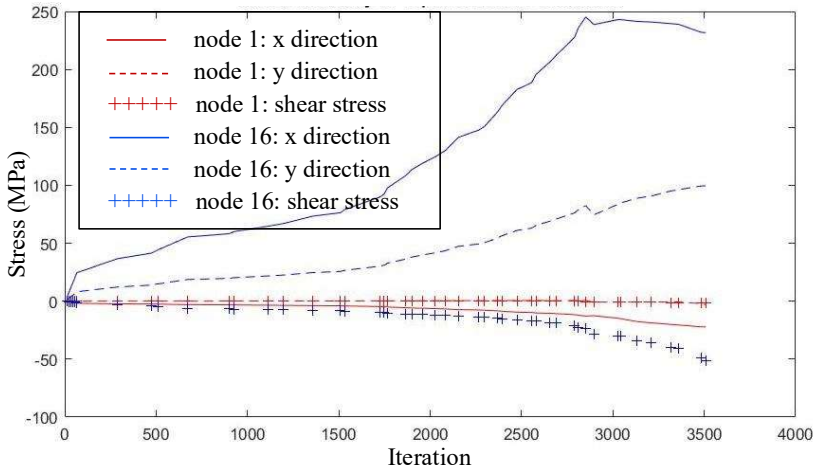


Fig. 11. Stress history of nodes 1 and 16 of the cantilever beam

Here, first the reinforcement reached its maximum capacity and maintained this capacity without increasing it, while the stress value in the concrete continued to develop and reached its maximum value. The stress value in the reinforcement here can be greater than the maximum stress value determined by uniaxial tests. The reason for this is that the reinforcement material model is followed through the equivalent stress value. As a matter of fact, when looking at the von Mises stress diagram (Fig. 12c), it is seen that the highest stress value in the reinforcement reaches the reinforcement capacity value approximately after the 2800th iteration and is closer to the capacity value than the stress value in the σ_{xx} diagram.

The cumulative plastic strain amounts of the cantilever beam were calculated for the integration point number 1 of the 1st element, and the values corresponding to the effective stress values are shown in Fig. 12d. For the capped Drucker-Prager model, the cumulative plastic strain and effective stress calculations are given in Eqs. 41-42. The equivalent plastic strain increase $\Delta\bar{\varepsilon}^p$ is mentioned in Eq. 10.

$$\bar{\varepsilon}^p_{n+1} = \bar{\varepsilon}^p_n + \Delta\bar{\varepsilon}^p \tag{41}$$

$$\sigma_{eff} = \frac{\alpha(\kappa)3p_{n+1} + \sqrt{J_2|s_{n+1}|}}{\alpha(\kappa) + \frac{1}{\sqrt{3}}} \tag{42}$$

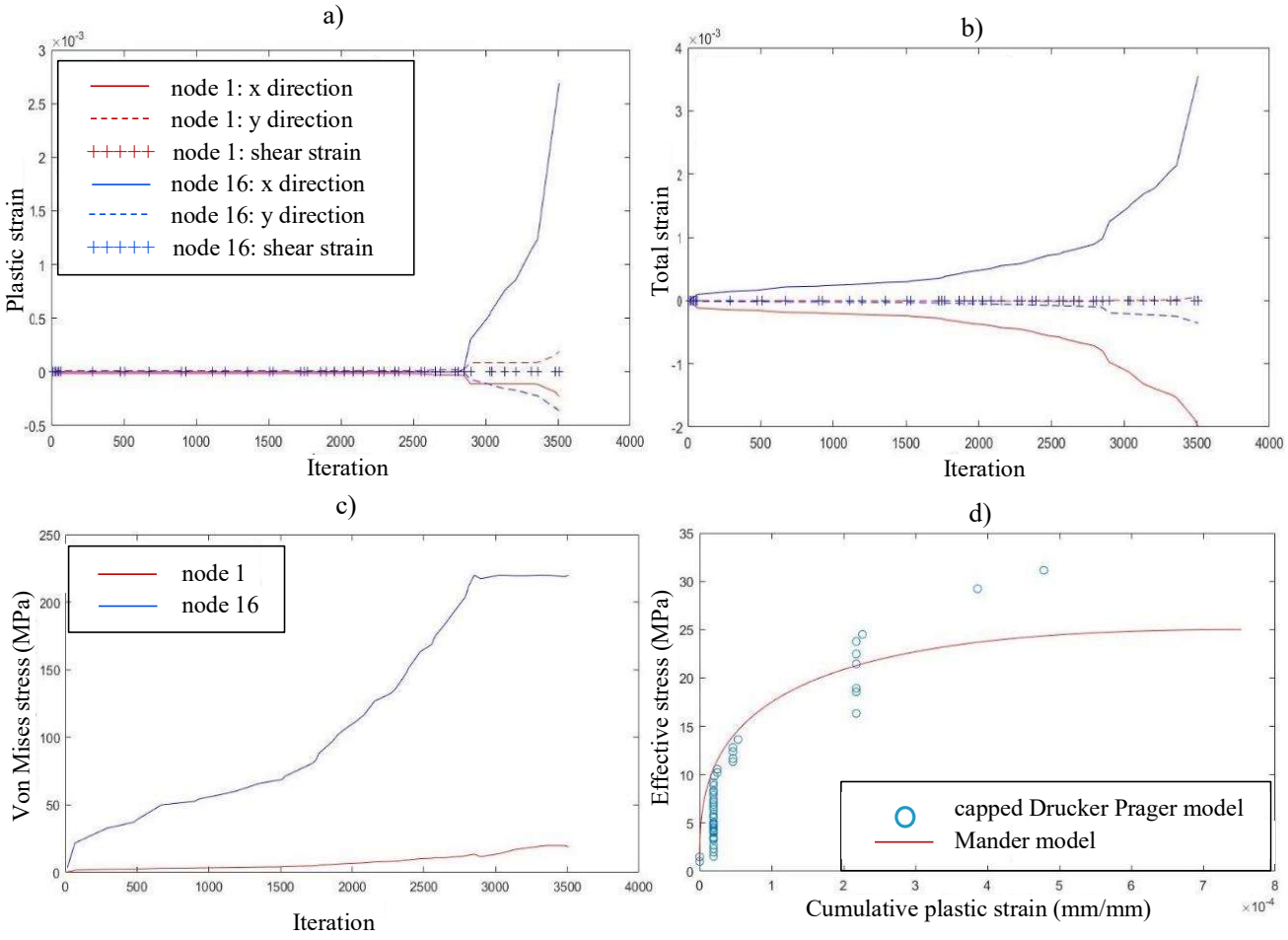


Fig. 12. a) Plastic strain history of nodes 1 and 16 of the cantilever beam, b) total strain history of nodes 1 and 16 of the cantilever beam, c) von Mises stress history of nodes 1 and 16 of the cantilever beam, d) cumulative plastic strain and effective stress relationship of cantilever beam

In the study, the change of bulk modulus with volumetric strain could not be obtained for the Mander model. For this reason, the bulk modulus (K) was accepted as constant. As seen in Fig. 13, it is seen that the bulk modulus changes in the studies. It can be thought that the deviations in the effective stress-cumulative plastic strain graph are caused by this situation. In addition, the tolerance value for convergence at the force level was taken as 10^{-2}. Reducing the tolerance can reduce the amount of these deviations.

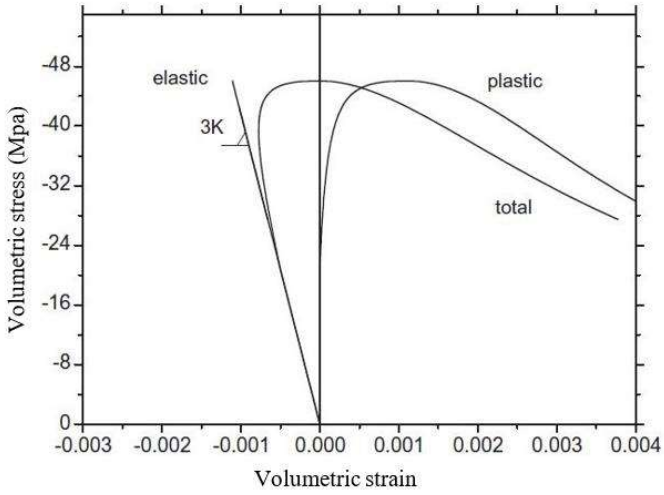


Fig. 13. Typical volumetric behavior of concrete under uniaxial compression (Carrazedo et al. 2013)

Fig. 14a shows the distribution of the damage amount calculated for all integration points of each element. Plastic strain distributions of the cantilever beam are shown in Fig. 14b,c and d.

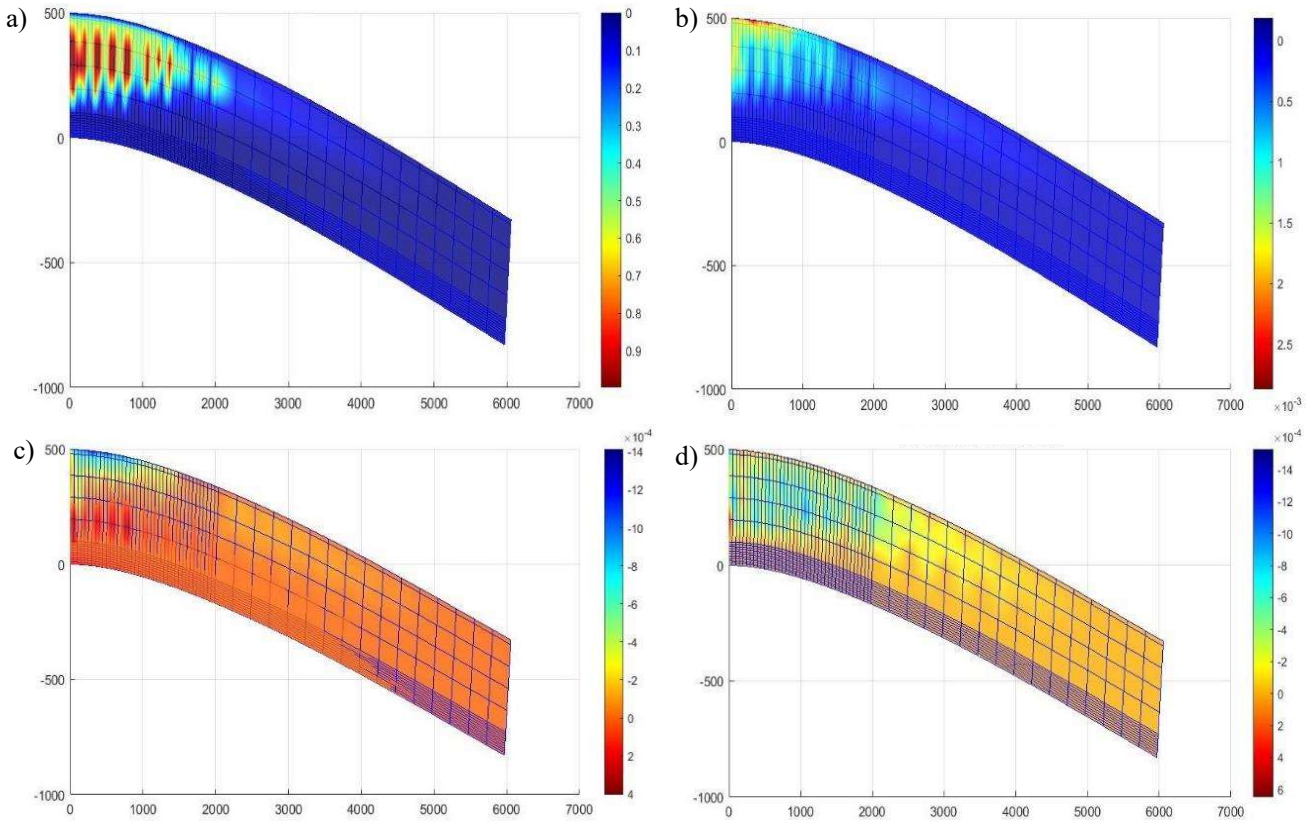


Fig. 14. a) Damage distribution in the concrete material of the cantilever beam, b) plastic strain distribution in the x-axis direction of the cantilever beam, c) plastic strain distribution in the y-axis direction of the cantilever beam, d) plastic shear strain distribution of cantilever beam

2.4.2. Reinforced concrete frame system

In this example, a reinforced concrete frame system with a width of 6000 mm and a height of 3000 mm is modeled. Column and beam sections were chosen with dimensions of 500x250 mm. Concrete and reinforcing steel material properties are taken as the same as the values in Table 1. 20 mm diameter reinforcements are positioned four at the top and bottom of the column, and inside and outside of the beams. The frame system is divided into rectangular finite elements consisting of 552 elements and 651 nodes. The relatively thin elements (20 mm) seen in Fig. 15 represent the reinforcement elements. A load combination of 340 kN from the upper left point of the system in the horizontal and 1250 kN from the middle point of the beam in the vertical is applied to the system. The Eq. 43 was used for lateral stiffness in a frame with beam length L, column height h, L = 2h, and column-beam bending resistances $EI_c = EI_b$ (Chopra, 2013).

$$k = \frac{96}{7}\frac{EI_c}{h^3} \tag{43}$$

In this regard, the column load carrying capacity, which is assumed to operate at 20% capacity, was calculated in Eq. 44 and was applied to the system as a singular load from the middle of the beam.

$$\frac{500 * 250 * 25}{1000} 2 * 0{,}20 = 1250\ kN \tag{44}$$

In line with the prepared program, the capped Drucker Prager yield surface for the frame system example is created as shown in Fig. 16.

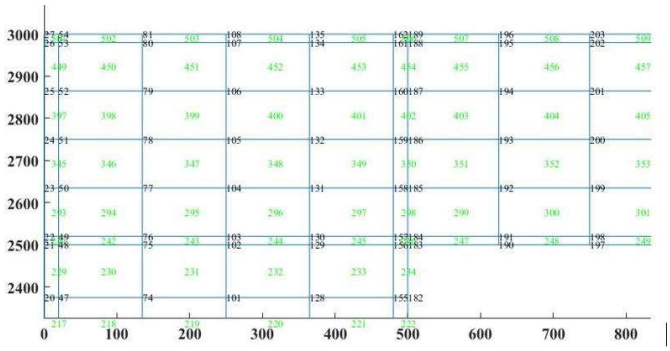


Fig. 15. A section from the finite element modeling of the frame system

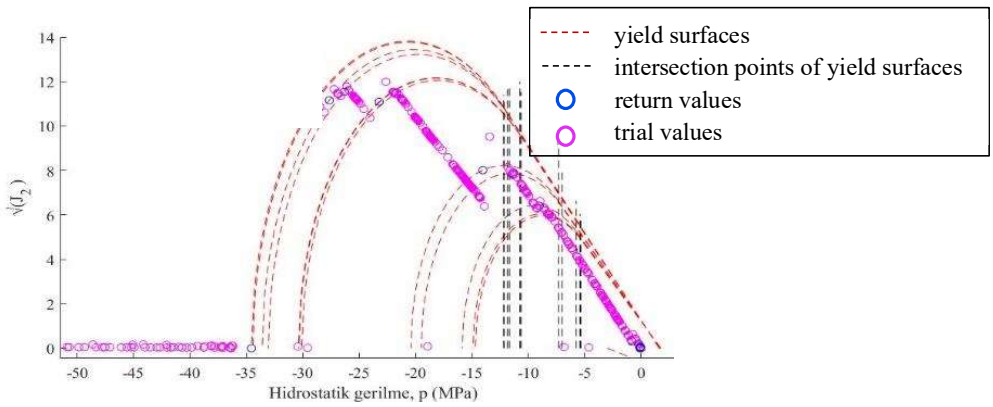


Fig. 16. Capped Drucker-Prager yield surface for frame system

The stress distributions of the cantilever beam analyzed with the specified loading are shown in Fig. 17. Looking at the shear stress distribution given in Fig. 17c, it can be seen that there is an antimetric distribution.

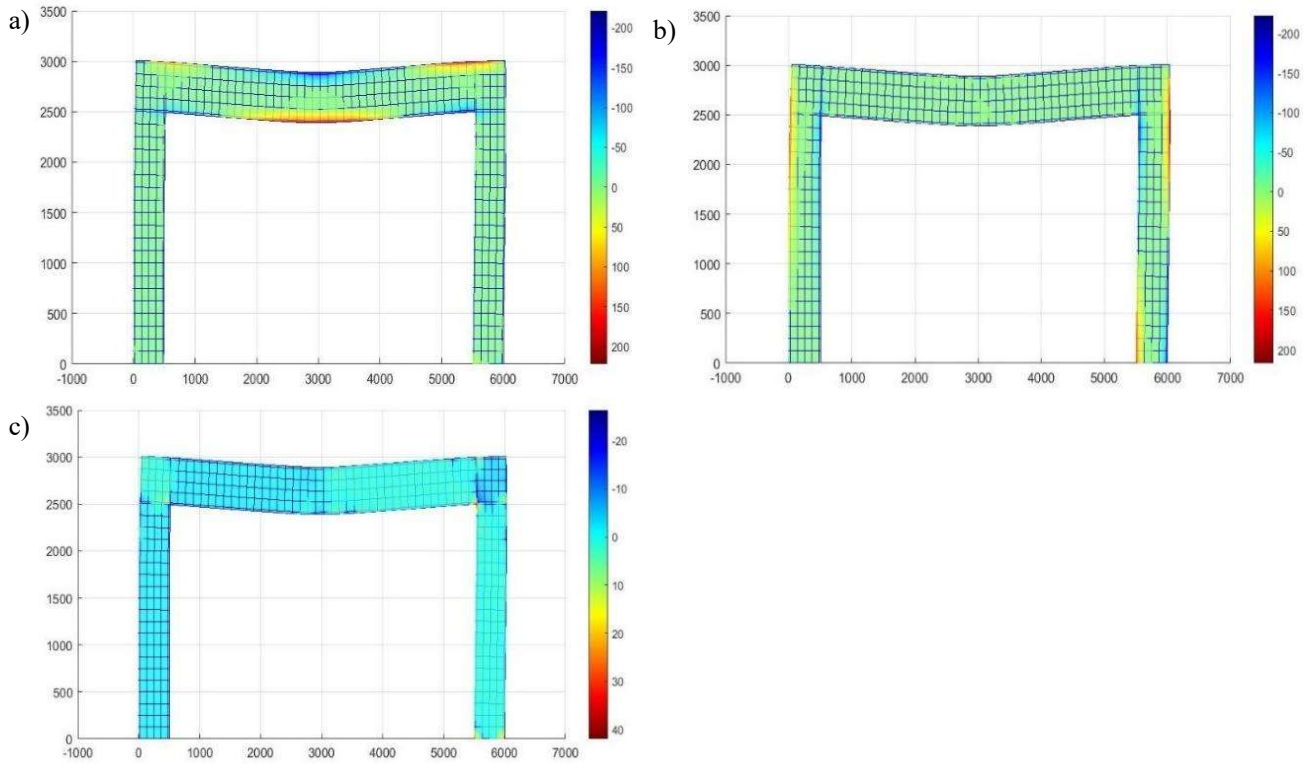


Fig. 17. a) Stress distribution in the x-axis direction of the frame system, b) stress distribution in the y-axis direction of the frame system, c) shear stress distribution of the frame system

Graphs on which stress and strains are drawn in the frame system are prepared for the nodes shown in Fig. 18.

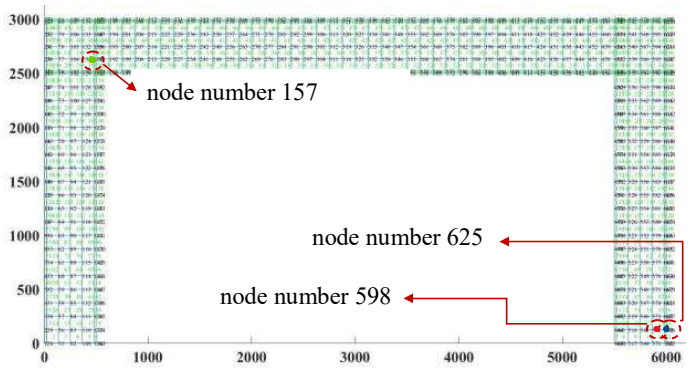


Fig. 18. Points observed in the frame system

As a result, the variation of the stress (Fig. 19a), plastic strain (Fig. 19b), total strain (Fig. 19c) and von Mises stress (Fig. 19d) of the node points 598, 625 and 157 of the system depending on the iterations are shown in the graphs below. Node 598 and 157 represents the concrete element and node 625 represents the reinforcement element (Fig. 18). The blue color belongs to the node number 625, the red color belongs to the node number 598 and the green color belongs to the node number 157.

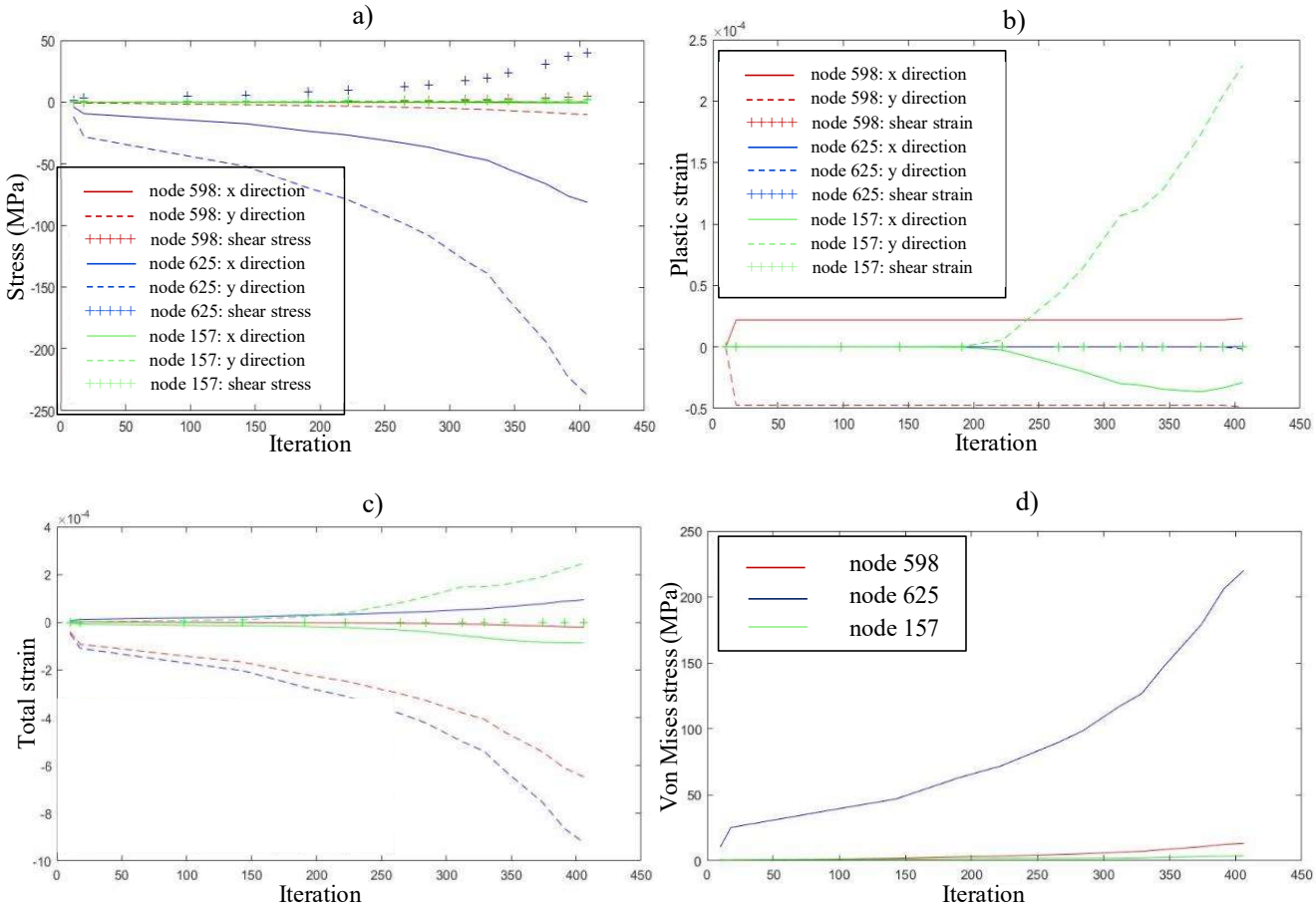


Fig. 19. a) Stress history of points 598, 625 and 157 of the frame system, b) plastic strain history of points 598, 625 and 157 of the frame system, c) total strain history of points 598, 625 and 157 of the frame system, d) von Mises stress history of points 598, 625 and 157 of the frame system

Cumulative plastic strain amounts of the frame system were calculated for the integration point number 2 of the 11th element (right column, lower right corner concrete element), and the values corresponding to the effective stress values are shown in Fig. 20.

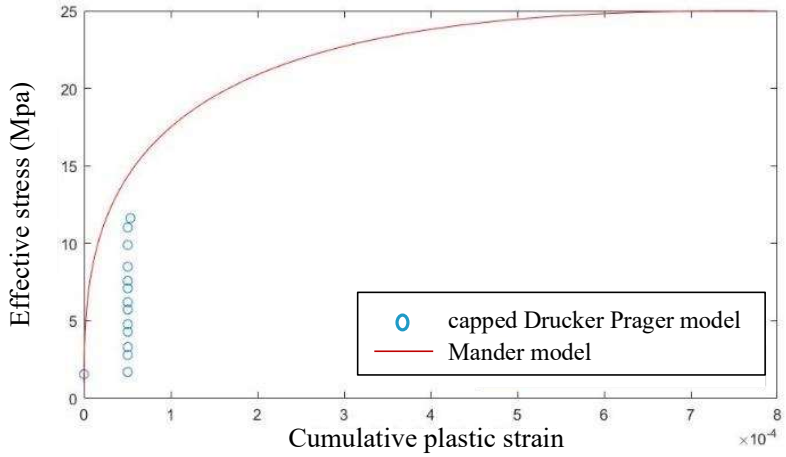


Fig. 20. Cumulative plastic strain and effective stress relationship of the frame system

Fig. 21a shows the distribution of the damage amount calculated for all integration points of each element. Plastic strain distributions of the frame system are shown in Fig. 21b, c and d.

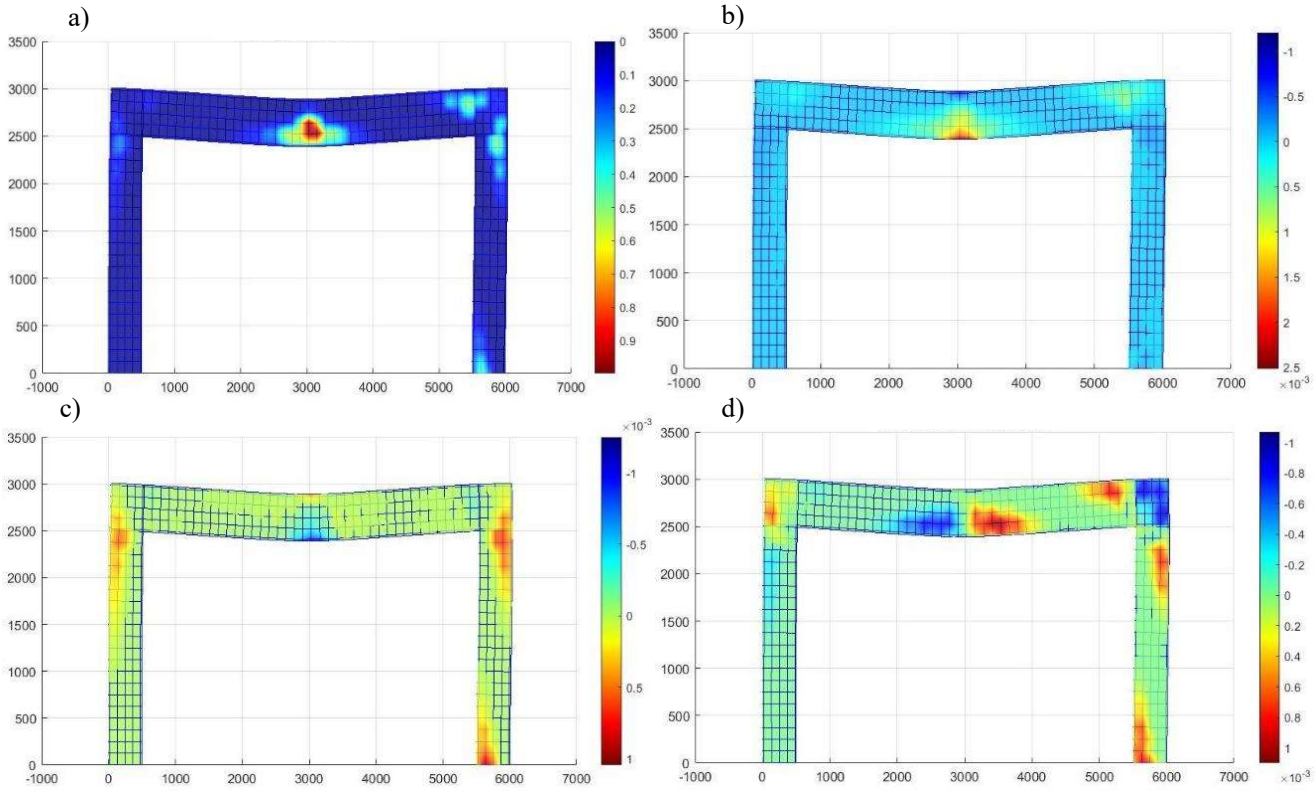


Fig. 21. a) Damage distribution in the concrete material of the frame system, b) plastic strain distribution in the x-axis direction of the frame system, c) plastic strain distribution in the y-axis direction of the frame system, d) plastic shear strain distribution of the frame system

As a result of the study, some generalizable results obtained from discussions on examples are given below:

- Maximum stress values were reached in the concrete and reinforcement elements in the solved samples.
- Yielding was observed in the reinforcement elements.
- The stress-strain curve of the Mander model could be followed to a reasonable extent. It is thought that the relatively large deviations in the graph are due to the step size in the Newton Raphson step.
- The cap region added to the Drucker-Prager model limits the yield surface in hydrostatic compression and helps control volume expansion. As seen in the analyzes and yield surface graphics, return algorithms also work on the cap region. This shows the necessity of the cap region.
- The change of the neutral axis along the section can be observed.
- In the study, the change of bulk modulus with volumetric strain could not be obtained for the Mander model. For this reason, the bulk modulus (K) was accepted as constant. It can be thought that the deviations in the effective stress-cumulative plastic strain graph are caused by this situation.

Declaration of conflicting interests

The author(s) declared no potential conflicts of interest with respect to the research, authorship, and/or publication of this article.

References

Auricchio F, Taylor RL (1999) A Return-map algorithm for general associative isotropic elasto-plastic materials in large deformation regimes. International Journal of Plasticity 15(12):1359-1378.

Carrazedo R, Mirmiran A, de Hanai JB (2013) Plasticity based stress–strain model for concrete confinement. Engineering Structures 48:645-657.

Chen WF (1982) Plasticity in Reinforced Concrete. New York:270-274.

Chopra AK (2013) Dynamics of Structures, Theory and Applications to Earthquake Engineering, 4th edition. Pearson, USA.

Ding X, Zhang G (2017) Coefficient of equivalent plastic strain based on the associated flow of the drucker-prager criterion. International Journal of Non-Linear Mechanics 93:15-20.

Drucker DC., Prager W (1952) Soil mechanics and plastic analysis or limit design. Quarterly of Applied Mathematics 10(2):157-165.

Hafezolghorani M, Hejazi F, Vaghei R, Jaafar MS, Karimzade K (2017) Simplified damage plasticity model for concrete. Structural Engineering International 27(1):68-78.

Hayrioğlu S, Bekiroğlu S (2022) Geliştirilmiş Sonlu Elemanlar Algoritmasi ile Düzlem Elasto-Plastik Betonarme Çerçeve Sisteminin Modellenmesi. MSc Dissertation, Yıldız Technical University (in Turkish).

Jirásek M, Bažant ZP (2002) Von Mises Criterion. Inelastic Analysis of Structure. West Sussex, England.

Mander B, Priestley MJN, Park R (1988) Theoretical stress-strain model for confined concrete. Journal of Structural Engineering 114(8):1804-1826.

Mirmiran A, Shahawy M (1997) Dilation characteristics of confined concrete. Mechanics of Cohesive-Frictional Materials 2(3):237-249.

Owen DRJ, de Souza Neto EA, Peric D (2008) Computational Methods for Plasticity Theory and Applications. Pearson, West Sussex.

Popovics S (1973) A Numerical approach to the complete stress-strain curve of concrete. Cement and Concrete Research 3:583-599.

TBEC (2018) Türkiye Building Earthquake Code: Rules for Design of Buildings under Earthquake Effect. Ankara (in Turkish).